Bicritical behavior of period doublings in unidirectionally coupled maps

Sang-Yoon Kim*

Department of Physics, Kangwon National University, Chunchon, Kangwon-Do 200-701, Korea
(Received 6 January 1999)

We study the scaling behavior of period doublings in two unidirectionally coupled one-dimensional maps near a bicritical point where two critical lines of period-doubling transition to chaos in both subsystems meet. Note that the bicritical point corresponds to a border of chaos in both subsystems. For this bicritical case, the second response subsystem exhibits a type of non-Feigenbaum critical behavior, while the first drive subsystem is in the Feigenbaum critical state. Using two different methods, we make the renormalization-group analysis of the bicritical behavior and find the corresponding fixed point of the renormalization transformation with two relevant eigenvalues. The scaling factors obtained by the renormalization-group analysis agree well with those obtained by a direct numerical method. [S1063-651X(99)02006-1]

I. INTRODUCTION

Period-doubling transition to chaos has been extensively studied in a one-parameter family of one-dimensional (1D) unimodal maps,

$$x_{t+1} = 1 - A x_t^2, \tag{1}$$

where x_t is a state variable at a discrete time t. As the control parameter A is increased, the 1D map undergoes an infinite sequence of period-doubling bifurcations accumulating at a critical point A_c, beyond which chaos sets in. Using a renormalization-group (RG) method, Feigenbaum [1] has discovered universal scaling behavior near the critical point A_c.

Here we are interested in the period doublings in a system consisting of two 1D maps with a one-way coupling,

$$x_{t+1} = 1 - A x_t^2, \quad y_{t+1} = 1 - B y_t^2 - C x_t^2, \tag{2}$$

where x and y are state variables of the first and second subsystems, A and B are control parameters of the subsystems, and C is a coupling parameter. Note that the first (drive) subsystem acts on the second (response) subsystem, while the second subsystem does not influence the first subsystem. This kind of unidirectionally coupled 1D maps have been used as a model for open flow systems [2]. In particular, such systems with unidirectional coupling are actively discussed recently in application to secure communication using synchronous chaos [3].

A kind of non-Feigenbaum scaling behavior was found in the unidirectionally coupled 1D maps (2) near a bicritical point (A_c, B_c) where two critical lines of period-doubling transition to chaos in both subsystems meet [4]. For this bicritical case, a RG analysis was also developed and the corresponding fixed point, governing the bicritical behavior, was numerically obtained by directly solving the RG fixed-point equation using a polynomial approximation [5]. In this paper, using two different methods, we also make the RG analysis of the bicriticality, the results of which agree well

with those of previous works. Note that this kind of non-Feigenbaum critical behavior was also found both in an electronic system of two periodically driven nonlinear LC circuits with a unidirectional coupling [4] and in a system of two unidirectionally coupled Chua's circuits [6]. It is thus believed that the bicriticality in the abstract system of the unidirectionally coupled 1D maps may be observed in a real system consisting of two period-doubling subsystems with a unidirectional coupling.

This paper is organized as follows. In Sec. II we study the scaling behavior near a bicritical point (A_c, B_c), corresponding to a border of chaos in both subsystems, by directly following a period-doubling sequence converging to the point (A_c, B_c) for a fixed value of C. For this bicritical case, a type of non-Feigenbaum critical behavior appears in the second subsystem, while the first subsystem is in the Feigenbaum critical state. Employing two different methods, we make the RG analysis of the bicritical behavior in Sec. III. To solve the RG fixed-point equation, we first use an approximate truncation method [7], corresponding to the lowest-order polynomial approximation. Thus we analytically obtain the fixed point, associated with the bicritical behavior, and its relevant eigenvalues. Compared with the previous numerical results [5], these analytic results are not bad as the lowest-order approximation. To improve accuracy, we also employ the "eigenvalue-matching" RG method [8], equating the stability multipliers of the orbit of level n (period 2^n) to those of the orbit of the next level $n + 1$. Thus we numerically obtain the bicritical point, the parameter and orbital scaling factors, and the critical stability multipliers. We note that the accuracy is improved remarkably with increasing the level n. Finally, a summary is given in Sec. IV.

II. SCALING BEHAVIOR NEAR THE BICRITICAL POINT

In this section we fix the value of the coupling parameter by setting $C = 0.45$ and directly follow a period-doubling sequence converging to the bicritical point (A_c, B_c), which corresponds to a border of chaos in both subsystems. For this bicritical case, the second subsystem exhibits a type of non-Feigenbaum critical behavior, while the first subsystem is in the Feigenbaum critical state.
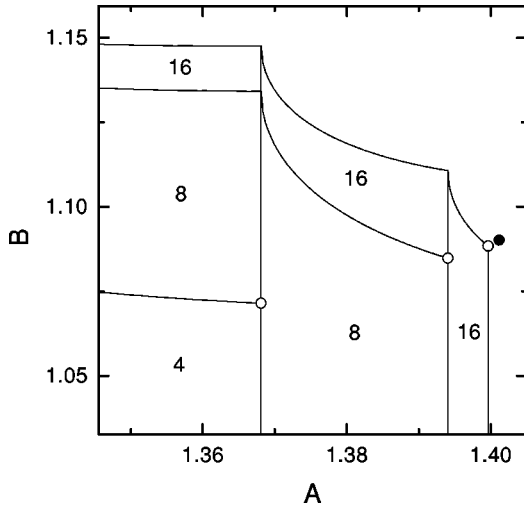
*Electronic address: sykim@cc.kangwon.ac.kr

FIG. 1. Stability diagram of the periodic orbits born via period-doubling bifurcations for $C=0.45$. The numbers in the different regions represent the period of motion in the second subsystem. The open circles also denote the point, corresponding to a threshold of instability in both subsystems, where $\lambda_1=-1$ and $\lambda_2=-1$. Such open circles accumulate to the bicritical point, denoted by the solid circle, which corresponds to a border of chaos in both subsystems. For other details, see the text.

The unidirectionally coupled 1D maps (2) may have many attractors for fixed values of the parameters [9]. For the case $C=0$, it breaks up into the two uncoupled 1D maps. If they both have stable orbits of period 2^k, then the composite system has 2^k different stable states distinguished by the phase shift between the subsystems. This multistability is preserved when the coupling is introduced, at least while its value is small enough. Here we study only the attractors whose basins include the origin $(0,0)$. Such attractors become in phase when $A=B$ and $C=0$.

Stability of an orbit with period q is determined by its stability multipliers,

$$\lambda_1=\prod_{t=1}^{q}(-2Ax_t), \quad \lambda_2=\prod_{t=1}^{q}(-2By_t). \quad (3)$$

Here λ_1 and λ_2 determine the stability of the first and second subsystems, respectively. An orbit becomes stable when the moduli of both multipliers are less than unity, i.e., $-1<\lambda_i<1$ for $i=1,2$.

Figure 1 shows the stability diagram of periodic orbits for $C=0.45$. As the parameter A is increased, the first subsystem exhibits a sequence of period-doubling bifurcations at the vertical straight lines, where $\lambda_1=-1$. For small values of the parameter B, the period of oscillation in the second subsystem is the same as that in the first subsystem, as in the case of forced oscillation. As B is increased for a fixed value of A, a sequence of period-doubling bifurcations occurs in the second subsystem when crossing the nonvertical lines where $\lambda_2=-1$. The numbers inside the different regions denote the period of the oscillation in the second subsystem.

We consider a pair of the parameters (A_n,B_n), at which the periodic orbit of level n (period 2^n) has the stability multipliers $\lambda_{1,n}=\lambda_{2,n}=-1$. Hence, the point (A_n,B_n) corresponds to a threshold of instability in both subsystems.

TABLE I. Sequences of the parameter and the orbit point, $\{B_n\}$ and $\{y_n\}$, in the second subsystem.

n	B_n	y_n
10	1.090 088 955 364	$5.019\,189\times10^{-3}$
11	1.090 092 109 910	$-3.333\,775\times10^{-3}$
12	1.090 093 416 851	$2.214\,467\times10^{-3}$
13	1.090 093 959 979	$-1.471\,024\times10^{-3}$
14	1.090 094 186 392	$9.771\,970\times10^{-4}$
15	1.090 094 280 906	$-6.491\,561\times10^{-4}$
16	1.090 094 320 376	$4.312\,391\times10^{-4}$
17	1.090 094 336 865	$-2.864\,762\times10^{-4}$
18	1.090 094 343 755	$1.903\,092\times10^{-4}$
19	1.090 094 346 634	$-1.264\,245\times10^{-4}$
20	1.090 094 347 837	$8.398\,518\times10^{-5}$
21	1.090 094 348 340	$-5.579\,230\times10^{-5}$

Some of such points are denoted by the open circles in Fig. 1. Then such a sequence of (A_n,B_n) converges to the bicritical point (A_c,B_c), corresponding to a border of chaos in both systems, with increasing the level n. The bicritical point is denoted by the solid circle in Fig. 1. To locate the bicritical point with a satisfactory precision, we numerically follow the orbits of period $q=2^n$ up to level $n=21$ in a quadruple precision, and obtain the sequences of both the parameters (A_n,B_n) and the orbit points (x_n,y_n) approaching the origin. We first note that the sequences of A_n and x_n in the first subsystem are the same as those in the 1D maps [1]. Hence, only the sequences of B_n and y_n in the second subsystem are given in Table I.

We now study the asymptotic scaling behavior of the period-doubling sequences in both subsystems near the bicritical point. The scaling behavior in the first subsystem is obviously the same as that in the 1D maps [1]. That is, the sequences $\{A_n\}$ and $\{x_n\}$ accumulate to their limit values, $A=A_c$ ($=1.401\,155\,189\,092\dots$) and $x=0$, geometrically as follows:

$$A_n-A_c\sim\delta_1^{-n}, \quad x_n\sim\alpha_1^{-n} \quad \text{for large } n. \quad (4)$$

The scaling factors δ_1 and α_1 are just the Feigenbaum constants δ ($=4.669\dots$) and α ($=-2.502\dots$) for the 1D maps, respectively. However, the second subsystem exhibits a non-Feigenbaum critical behavior, unlike the case of the first subsystem. The two sequences $\{B_n\}$ and $\{y_n\}$ also converge geometrically to their limit values $B=B_c$ ($=1.090\,094\,348\,701$) and $y=0$, respectively, where the value of B_c is obtained using the superconverging method [10]. To obtain the convergence rates of the two sequences, we define the scaling factors of level n:

$$\delta_{2,n}\equiv\frac{B_{n-1}-B_n}{B_n-B_{n+1}}, \quad \alpha_{2,n}\equiv\frac{y_{n-1}-y_n}{y_n-y_{n+1}}. \quad (5)$$

These two sequences $\{\delta_{2,n}\}$ and $\{\alpha_{2,n}\}$ are listed in Table II, and they converge to their limit values,

$$\delta_2\approx2.3928, \quad \alpha_2\approx-1.5053, \quad (6)$$

TABLE II. Sequences of the parameter and orbital scaling factors, $\{\delta_{2,n}\}$ and $\{\alpha_{2,n}\}$, in the second subsystem.

n	$\delta_{2,n}$	$\alpha_{2,n}$
10	2.429 8	−1.505 733 1
11	2.413 7	−1.505 515 4
12	2.406 3	−1.505 428 1
13	2.398 8	−1.505 375 3
14	2.395 6	−1.505 344 0
15	2.394 6	−1.505 331 6
16	2.393 7	−1.505 325 6
17	2.393 1	−1.505 321 5
18	2.393 0	−1.505 319 8
19	2.392 9	−1.505 319 1
20	2.392 8	−1.505 318 6

respectively. Note that these scaling factors are completely different from those in the first subsystem (i.e., the Feigenbaum constants for the 1D maps).

For evidence of scaling, we compare the chaotic attractors, shown in Fig. 2, for the three values of (A,B) near the bicritical point (A_c,B_c). All these attractors are the hyperchaotic ones with two positive Lyapunov exponents [11],

$$\sigma_1 = \lim_{m\to\infty} \frac{1}{m} \sum_{t=1}^{m} \ln|2Ax_t|, \quad \sigma_2 = \lim_{m\to\infty} \frac{1}{m} \sum_{t=1}^{m} \ln|2By_t|.$$

(7)

Here the first and second Lyapunov exponents σ_1 and σ_2 denote the average exponential divergence rates of nearby orbits in the first and second subsystems, respectively. Figure 2(a) shows the hyperchaotic attractor with $\sigma_1 \simeq 0.242$ and $\sigma_2 \simeq 0.04$ for $A = A_c + \Delta A$ and $B = B_c + \Delta B$, where $\Delta A = \Delta B = 0.1$. This attractor consists of two pieces. To see scaling, we first rescale ΔA and ΔB with the parameter scaling factors δ_1 and δ_2, respectively. The attractor for the rescaled parameter values of $A = A_c + \Delta A/\delta_1$ and $B = B_c + \Delta B/\delta_2$ is shown in Fig. 2(b). It is also the hyperchaotic attractor with $\sigma_1 \simeq 0.121$ and $\sigma_2 \simeq 0.02$. We next magnify the region in the small box (containing the origin) by the scaling factor α_1 for the x axis and α_2 for the y axis, and then we get the picture in Fig. 2(c). Note that the picture in Fig. 2(c) reproduces the previous one in Fig. 2(a) approximately. Repeating the above procedure once more, we obtain the two pictures in Figs. 2(d) and 2(e). That is, Fig. 2(d) shows the hyperchaotic attractor with $\sigma \simeq 0.061$ and $\sigma_2 \simeq 0.01$ for $A = A_c + \Delta A/\delta_1^2$ and $B = B_c + \Delta B/\delta_2^2$. Magnifying the region in the small box with the scaling factors α_1^2 for the x axis and α_2^2 for the y axis, we also obtain the picture in Fig. 2(e), which reproduces the previous one in Fig. 2(c) with an increased accuracy.

So far we have seen the scaling near the bicritical point, and now turn to a discussion of the behavior exactly at the bicritical point (A_c,B_c). There exist an infinity of unstable periodic orbits with period 2^n at the bicritical point. The orbit points x_n and y_n, approaching the zero in the first and second subsystems, vary asymptotically in proportion to α_1^{-n} and α_2^{-n}, respectively. The stability multipliers $\lambda_{1,n}$ and $\lambda_{2,n}$ of the orbits with period 2^n also converge to the critical
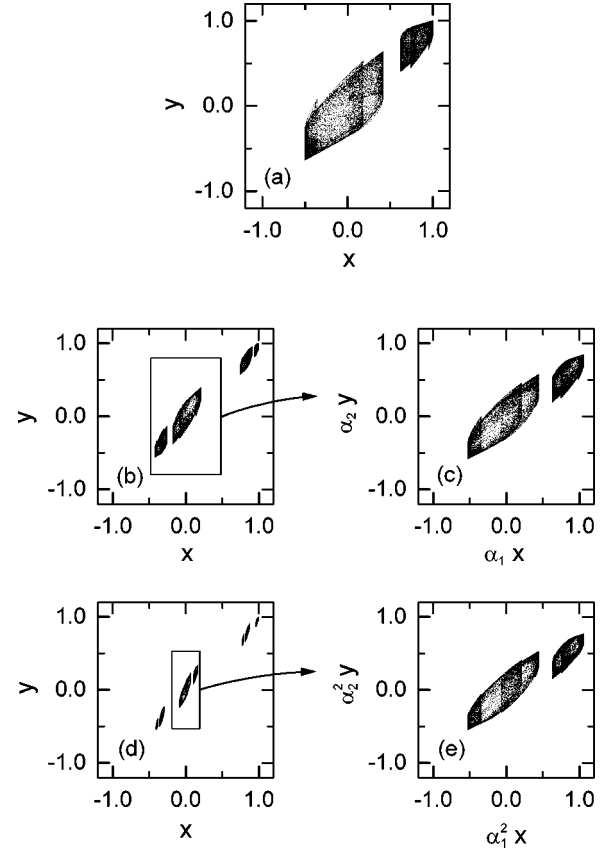

FIG. 2. Hyperchaotic attractors for the three values of (A,B) near the bicritical point $(A_c.B_c)$; in (a) $(A,B)=(A_c+\Delta A, B_c+\Delta B)$ $(\Delta A=\Delta B=0.1)$, in (b) and (c) $(A,B)=(A_c+\Delta A/\delta_1, B_c+\Delta B/\delta_2)$, and in (d) and (e) $(A,B)=(A_c+\Delta A/\delta_1^2, B_c+\Delta B/\delta_2^2)$. The picture in (c) is obtained by magnifying the region in the small box in (b) with the scaling factors α_1 for the x axis and α_2 for the y axis. Similarly, we also obtain the picture (e) by magnifying the region inside the small box in (d) with the scaling factors α_1^2 for the x axis and α_2^2 for the y axis. Comparing the pictures in (a), (c), and (e), one can see that each successive magnified picture reproduces the previous one with an accuracy with the depth of resolution.

stability multipliers λ_1^* and λ_2^*, respectively. Here λ_1^* $(=-1.601\,191\,\ldots)$ in the first subsystem is just the critical stability multiplier for the case of the 1D maps [1]. However, as listed in Table III, the second subsystem has the different

TABLE III. Sequences of the second-stability multipliers, $\{\lambda_{2,n}\}$ of the orbits with period 2^n at the bicritical point.

n	$\lambda_{2,n}$
10	−1.178 829
11	−1.178 842
12	−1.178 839
13	−1.178 850
14	−1.178 855
15	−1.178 854
16	−1.178 854
17	−1.178 855
18	−1.178 855
19	−1.178 854

critical stability multiplier,

$$\lambda_2^* = -1.178\,85\,\ldots. \tag{8}$$

Consequently, the periodic orbits at the bicritical point have the same stability multipliers λ_1^* and λ_2^* for sufficiently large n.

III. RENORMALIZATION-GROUP ANALYSIS OF THE BICRITICAL BEHAVIOR

Employing two different methods, we make the RG analysis of the bicritical behavior. We first use the truncation method, and analytically obtain the corresponding fixed point and its relevant eigenvalues. These analytic results are not bad as the lowest-order approximation. To improve the accuracy, we also use the numerical eigenvalue-matching method, and obtain the bicritical point, the parameter and orbital scaling factors, and the critical stability multipliers. Note that the accuracy in the numerical RG results is improved remarkably with increasing the level n.

A. Truncation method

In this subsection, employing the truncation method [7], we analytically make the RG analysis of the bicritical behavior in the unidirectionally coupled map T of the form,

$$T: \quad x_{t+1} = f(x_t), \quad y_{t+1} = g(x_t, y_t), \tag{9}$$

where x_t and y_t are the state variables at a discrete time t in the first and second subsystems, respectively. Truncating the map (9) at its quadratic terms, we have

$$T_{\mathbf{P}}: \quad x_{t+1} = \frac{a}{b} + bx_t^2, \quad y_{t+1} = \frac{c}{d} + dy_t^2 + \frac{e}{d}x_t^2, \tag{10}$$

which is a five-parameter family of unidirectionally coupled maps. $\mathbf{P}$ represents the five parameters, i.e., $\mathbf{P} = (a,b,c,d,e)$. The construction of Eq. (10) corresponds to a truncation of the infinite dimensional space of unidirectionally coupled maps to a five-dimensional space. The parameters a, b, c, d, and e can be regarded as the coordinates of the truncated space. We also note that this truncation method corresponds to the lowest-order polynomial approximation.

We look for fixed points of the renormalization operator $\mathcal{R}$ in the truncated five-dimensional space of unidirectionally coupled maps,

$$\mathcal{R}(T) = \Lambda T^2 \Lambda^{-1}. \tag{11}$$

Here the rescaling operator Λ is given by

$$\Lambda = \begin{pmatrix} \alpha_1 & 0 \\ 0 & \alpha_2 \end{pmatrix}, \tag{12}$$

where α_1 and α_2 are the rescaling factors in the first and second subsystems, respectively.

The operation $\mathcal{R}$ in the truncated space can be represented by a transformation of parameters, i.e., a map from $\mathbf{P} \equiv (a,b,c,d,e)$ to $\mathbf{P}' \equiv (a',b',c',d',e')$,

$$a' = 2a^2(1+a), \tag{13a}$$

$$b' = \frac{2}{\alpha_1} ab, \tag{13b}$$

$$c' = 2c \left(c + c^2 + e\frac{a^2}{b^2} \right), \tag{13c}$$

$$d' = \frac{2}{\alpha_2} cd, \tag{13d}$$

$$e' = \frac{4}{\alpha_1^2} ce(a+c). \tag{13e}$$

The fixed point $\mathbf{P}^* = (a^*,b^*,c^*,d^*,e^*)$ of this map can be determined by solving $\mathbf{P}' = \mathbf{P}$. The parameters b and d set only the scales in the x and y, respectively, and thus they are arbitrary. We now fix the scales in x and y by setting $b = d = 1$. Then, we have, from Eqs. (13a)–(13e), five equations for the five unknowns $\alpha_1, a^*, \alpha_2, c^*$, and e^*. We thus find one solution, associated with the bicritical behavior, as will be seen below. The map (10) with a solution $\mathbf{P}^*$ ($T_{\mathbf{P}^*}$) is the fixed map of the renormalization transformation $\mathcal{R}$; for brevity $T_{\mathbf{P}^*}$ will be denoted as T^*.

We first note that Eqs. (13a) and (13b) are only for the unknowns α_1 and a^*. We find one solution for α_1 and a^*, associated with the period-doubling bifurcation in the first subsystem,

$$\alpha_1 = -1 - \sqrt{3} = -2.732\ldots, \quad a^* = \frac{\alpha_1}{2}. \tag{14}$$

Substituting the values for α_1 and a^* into Eqs. (13c)–(13e), we obtain one solution for α_2, c^*, and e^*, associated with the bicriticality,

$$\alpha_2 = \frac{1}{2}(1 + \sqrt{3} - \sqrt{5} - \sqrt{15}) = -1.688\ldots, \tag{15a}$$

$$c^* = \frac{\alpha_2}{2}, \quad e^* = 1 + \frac{1}{2}(\sqrt{15} - 3\sqrt{3}) = 0.338\ldots. \tag{15b}$$

Consider an infinitesimal perturbation $\epsilon\delta\mathbf{P}$ to a fixed point $\mathbf{P}^*$ of the transformation of parameters (13a)–(13e). Linearizing the transformation at $\mathbf{P}^*$, we obtain the equation for the evolution of $\delta\mathbf{P}$,

$$\delta\mathbf{P}' = J\delta\mathbf{P}, \tag{16}$$

where J is the Jacobian matrix of the transformation at $\mathbf{P}^*$.

The 5×5 Jacobian matrix J has a semiblock form, because we are considering the unidirectionally coupled case. Therefore, one can easily obtain its eigenvalues. The first two eigenvalues, associated with the first subsystem, are those of the following 2×2 matrix,

$$M_1 = \frac{\partial(a',b')}{\partial(a,b)}\bigg|_{P*} = \begin{pmatrix} 3-\alpha_1 & 0 \\ 2/\alpha_1 & 1 \end{pmatrix}. \tag{17}$$

Hence, the two eigenvalues of M_1, δ_1, and δ_1', are given by

$$\delta_1 = 4 + \sqrt{3} = 5.732\ldots, \qquad \delta_1' = 1. \tag{18}$$

$$M_2 = \frac{\partial(c',d',e')}{\partial(c,d,e)}\bigg|_{P*} = \begin{pmatrix} 4c*+6c*^2+2a*^2e* & 0 & 2a*^2c* \\ 2/\alpha_2 & 2c*/\alpha_2 & 0 \\ 4e*(a*+2c*)/\alpha_1^2 & 0 & 4c*(a*+c*)/\alpha_1^2 \end{pmatrix}. \tag{19}$$

The three eigenvalues of M_2, δ_2, δ_2', and δ_2'', are given by

$$\delta_2 = (u + \sqrt{v})/2 = 3.0246\ldots, \tag{20a}$$

$$\delta_2' = (u - \sqrt{v})/2 = 0.1379\ldots, \qquad \delta_2'' = 1, \tag{20b}$$

where

$$u = (17 + 7\sqrt{3} - 5\sqrt{5} - 3\sqrt{15})/2, \tag{21a}$$

$$v = 104 + 53\sqrt{3} - 44\sqrt{5} - 23\sqrt{15}. \tag{21b}$$

The first eigenvalue δ_2 is a relevant eigenvalue, associated with the scaling of the control parameter in the second subsystem, the second eigenvalue δ_2' is an irrelevant one, and the third eigenvalue δ_2'' is a marginal eigenvalue, associated with the scale change in y.

As shown in Sec. II, stability multipliers of an orbit with period 2^n at the bicritical point converge to the critical stability multipliers λ_1^* and λ_2^* as $n \to \infty$. We now obtain these critical stability multipliers analytically. The invariance of the fixed map $T*$ under the renormalization transformation $\mathcal{R}$ implies that, if $T*$ has a periodic point (x,y) with period 2^n, then $\Lambda^{-1}(x,y)$ is a periodic point of $T*$ with period 2^{n+1}. Since rescaling does not affect the stability multipliers, all the orbits with period 2^n ($n = 0,1,2,\ldots$) have the same stability multipliers, which are just the critical stability multipliers λ_1^* and λ_2^*. That is, the critical stability multipliers have the values of the stability multipliers of the fixed point $(x*,y*)$ of the fixed map $T*$,

$$\lambda_1^* = 2x* = -1.5424\ldots, \qquad \lambda_2^* = 2y* = -0.8899\ldots, \tag{22}$$

where

$$x* = (1 - \sqrt{3 + 2\sqrt{3}})/2, \qquad y* = (1 - \sqrt{w})/2, \tag{23a}$$

$$w = 5 + 3\sqrt{3} - 2\sqrt{5} - \sqrt{15} + \sqrt{3 + 2\sqrt{3}}(2 - 3\sqrt{3} + \sqrt{15}). \tag{23b}$$

Finally, we compare the analytic results for α_1, α_2, δ_1, δ_2, λ_1^*, and λ_2^* with the numerical values obtained in Sec. II, and find that the analytic ones are not bad as the lowest-order approximation.

Here the relevant eigenvalue δ_1 is associated with the scaling of the control parameter in the first subsystem, while the marginal eigenvalue δ_1' is associated with the scale change in x.

The remaining three eigenvalues, associated with the second subsystem, are those of the following 3×3 matrix,

B. Eigenvalue-matching method

In this subsection, we employ the eigenvalue-matching method [8] and numerically make the RG analysis of the bicritical behavior in the unidirectionally coupled map T of Eq. (2). As the level n increases, the accuracy in the numerical RG results are remarkably improved.

The basic idea is to associate a value (A',B') for each (A,B) such that $T_{(A',B')}^{(n+1)}$ locally resembles $T_{(A,B)}^{(n)}$, where $T^{(n)}$ is the 2^nth-iterated map of T (i.e., $T^{(n)} = T^{2^n}$). A simple way to implement this idea is to linearize the maps in the neighborhood of their respective fixed points and equate the corresponding eigenvalues.

Let $\{z_t\}$ and $\{z_t'\}$ be two successive cycles of period 2^n and 2^{n+1}, respectively, i.e.,

$$z_t = T_{(A,B)}^{(n)}(z_t), \qquad z_t' = T_{(A',B')}^{(n+1)}(z_t'); \qquad z_t = (x_t,y_t). \tag{24}$$

Here x_t depends only on A, but y_t is dependent on both A and B, i.e., $x_t = x_t(A)$ and $y_t = y_t(A,B)$. Then their linearized maps at z_t and z_t' are given by

$$DT_{(A,B)}^{(n)} = \prod_{t=1}^{2^n} DT_{(A,B)}(z_t), \tag{25a}$$

$$DT_{(A',B')}^{(n+1)} = \prod_{t=1}^{2^{n+1}} DT_{(A',B')}(z_t'). \tag{25b}$$

(Here DT is the linearized map of T.) Let their eigenvalues, called the stability multipliers, be $[\lambda_{1,n}(A),\lambda_{2,n}(A,B)]$ and $[\lambda_{1,n+1}(A'),\lambda_{2,n+1}(A',B')]$. The recurrence relations for the old and new parameters are then given by equating the stability multipliers of level n, $\lambda_{1,n}(A)$ and $\lambda_{2,n}(A,B)$, to those of the next level $n+1$, $\lambda_{1,n+1}(A')$ and $\lambda_{2,n+1}(A',B')$, i.e.,

$$\lambda_{1,n}(A) = \lambda_{1,n+1}(A'), \tag{26a}$$

$$\lambda_{2,n}(A,B) = \lambda_{2,n+1}(A',B'). \tag{26b}$$

The fixed point $(A*,B*)$ of the renormalization transformation (26),

$$\lambda_{1,n}(A*) = \lambda_{1,n+1}(A*), \tag{27a}$$

$$\lambda_{2,n}(A*,B*) = \lambda_{2,n+1}(A*,B*), \tag{27b}$$

gives the bicritical point (A_c, B_c). By linearizing the renormalization transformation (26) at the fixed point $(A*, B*)$, we have

$$\begin{pmatrix} \Delta A \\ \Delta B \end{pmatrix} = \begin{pmatrix} \left.\dfrac{\partial A}{\partial A'}\right|_* & \left.\dfrac{\partial A}{\partial B'}\right|_* \\ \left.\dfrac{\partial B}{\partial A'}\right|_* & \left.\dfrac{\partial B}{\partial B'}\right|_* \end{pmatrix} \begin{pmatrix} \Delta A' \\ \Delta B' \end{pmatrix} \tag{28}$$

$$= \Delta_n \begin{pmatrix} \Delta A' \\ \Delta B' \end{pmatrix}, \tag{29}$$

where $\Delta A = A - A*$, $\Delta B = B - B*$, $\Delta A' = A' - A*$, $\Delta B' = B' - B*$, and

$$\Delta_n = \Gamma_n^{-1} \Gamma_{n+1}, \tag{30a}$$

$$\Gamma_n = \begin{pmatrix} \left.\dfrac{d\lambda_{1,n}}{dA}\right|_* & 0 \\ \left.\dfrac{\partial\lambda_{2,n}}{\partial A}\right|_* & \left.\dfrac{\partial\lambda_{2,n}}{\partial B}\right|_* \end{pmatrix}, \tag{30b}$$

$$\Gamma_{n+1} = \begin{pmatrix} \left.\dfrac{d\lambda_{1,n+1}}{dA'}\right|_* & 0 \\ \left.\dfrac{\partial\lambda_{2,n+1}}{\partial A'}\right|_* & \left.\dfrac{\partial\lambda_{2,n+1}}{\partial B'}\right|_* \end{pmatrix}. \tag{30c}$$

Here Γ_n^{-1} is the inverse of Γ_n and the asterisk denotes the fixed point $(A*, B*)$. After some algebra, we obtain the analytic formulas for the eigenvalues $\delta_{1,n}$ and $\delta_{2,n}$ of the matrix Δ_n,

$$\delta_{1,n} = \dfrac{\left.\dfrac{d\lambda_{1,n+1}}{dA'}\right|_*}{\left.\dfrac{d\lambda_{1,n}}{dA}\right|_*}, \tag{31a}$$

$$\delta_{2,n} = \dfrac{\left.\dfrac{\partial\lambda_{2,n+1}}{\partial B'}\right|_*}{\left.\dfrac{\partial\lambda_{2,n}}{\partial B}\right|_*}. \tag{31b}$$

As $n \to \infty$, $\delta_{1,n}$ and $\delta_{2,n}$ approach δ_1 and δ_2, which are just the parameter scaling factors in the first and second subsystems, respectively. Note also that as in the 1D case, the local rescaling factors of the state variables are simply given by

$$\alpha_{1,n} = \left.\dfrac{dx}{dx'}\right|_* = \dfrac{\delta_{1,n}}{t_{1,n}}, \tag{32a}$$
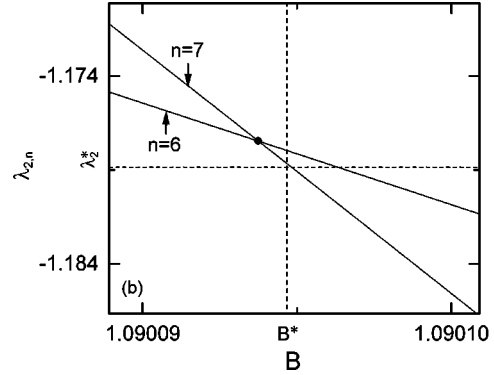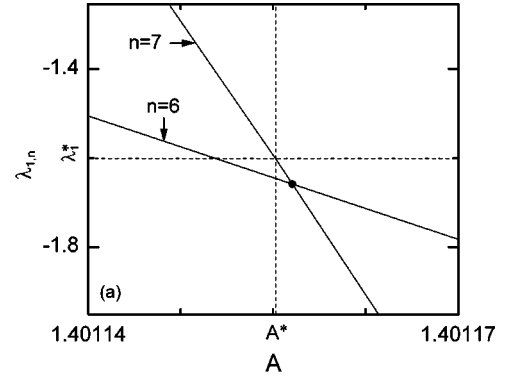

FIG. 3. Plots of (a) the first stability multipliers $\lambda_{1,n}(A)$ versus A and (b) the second stability multipliers $\lambda_{2,n}(A_6^*,B)$ versus B for the cases $n = 6,7$. In (a), the intersection point, denoted by the solid circle, of the two curves $\lambda_{1,6}$ and $\lambda_{1,7}$ gives the point $(A_6^*,\lambda_{1,6}^*)$ of level 6. As $n \to \infty$, $(A_n^*,\lambda_{1,n}^*)$ converges to its limit point $(A*,\lambda_1^*)$. Similarly, in (b), the intersection point, denoted also by the solid circle, of the two successive curves $\lambda_{2,6}(A_6^*,B)$ and $\lambda_{2,7}(A_6^*,B)$ gives the point $(B_6^*,\lambda_{2,6}^*)$ of level 6. As $n \to \infty$, $(B_n^*,\lambda_{2,n}^*)$ also approaches its limit point $(B*,\lambda_2^*)$. For other details, see the text.

$$\alpha_{2,n} = \left.\dfrac{dy}{dy'}\right|_* = \dfrac{\delta_{2,n}}{t_{2,n}}, \tag{32b}$$

where

$$t_{1,n} = \dfrac{\left.\dfrac{dx'}{dA'}\right|_*}{\left.\dfrac{dx}{dA}\right|_*}, \quad t_{2,n} = \dfrac{\left.\dfrac{\partial y'}{\partial B'}\right|_*}{\left.\dfrac{\partial y}{\partial B}\right|_*}. \tag{33}$$

Here $\alpha_{1,n}$ and $\alpha_{2,n}$ also converge to the orbital scaling factors, α_1 and α_2, in the first and second subsystems, respectively.

Some results for an intermediate level n are shown in Fig. 3. Figure 3(a) shows the plots of the first stability multiplier $\lambda_{1,n}(A)$ versus A for the cases $n = 6,7$. We note that the intersection point, denoted by the solid circle, of the two curves $\lambda_{1,6}$ and $\lambda_{1,7}$ gives the point $(A_6^*,\lambda_{1,6}^*)$ of level 6, where A_6^* and $\lambda_{1,6}^*$ are the critical point and the critical stability multiplier in the first subsystem, respectively. As the level n increases, A_n^* and $\lambda_{1,n}^*$ approach their limit values $A*$ and λ_1^*, respectively. Note also that the ratio of the slopes of the curves, $\lambda_{1,6}(A)$ and $\lambda_{1,7}(A)$, for $A = A_6^*$ gives the

TABLE IV. Sequences of the critical point, the first critical stability multiplier, the parameter and orbital scaling factors, $\{A_n^*\}$, $\{\lambda_{1,n}^*\}$, $\{\delta_{1,n}\}$ and $\{\alpha_{1,n}\}$, in the first subsystem. For comparison, we also list the results obtained by a direct numerical method in the last row.

n	A_n^*	$\lambda_{1,n}^*$	$\delta_{1,n}$	$\alpha_{1,n}$
6	1.401 155 189 088 929 1	-1.601 191 211 121 2	4.669 203 072 1	-2.502 620 459 5
7	1.401 155 189 092 133 2	-1.601 191 342 517 1	4.669 201 428 5	-2.502 845 988 3
8	1.401 155 189 092 048 4	-1.601 191 326 288 7	4.669 201 631 4	-2.502 894 652 0
9	1.401 155 189 092 050 7	-1.601 191 328 294 3	4.669 201 606 3	-2.502 905 037 7
10	1.401 155 189 092 050 6	-1.601 191 328 046 4	4.669 201 609 4	-2.502 907 267 8
11	1.401 155 189 092 050 6	-1.601 191 328 077 0	4.669 201 609 1	-2.502 907 744 9
12	1.401 155 189 092 050 6	-1.601 191 328 073 2	4.669 201 609 1	-2.502 907 847 2
13	1.401 155 189 092 050 6	-1.601 191 328 073 7	4.669 201 609 1	-2.502 907 869 1
14	1.401 155 189 092 050 6	-1.601 191 328 073 6	4.669 201 609 1	-2.502 907 873 8
15	1.401 155 189 092 050 6	-1.601 191 328 073 6	4.669 201 609 1	-2.502 907 874 8
	1.401 155 189 092 050 6	-1.601 191 328 073 6	4.669 201 609 1	-2.502 907 875 1

parameter scaling factor $\delta_{1,6}$ of level 6 in the first subsystem. Similarly, Fig. 3(b) shows the plots of the second stability multiplier $\lambda_{2,n}(A_6^*,B)$ versus B for the cases $n=6,7$. The intersection point, denoted also by the solid circle, of the two curves $\lambda_{2,6}(A_6^*,B)$ and $\lambda_{2,7}(A_6^*,B)$ gives the point $(B_6^*,\lambda_{2,6}^*)$ of level 6, where B_6^* and $\lambda_{2,6}^*$ are the critical point and the critical stability multiplier in the second subsystem, respectively. As the level n increases, B_n^* and $\lambda_{2,n}^*$ also converge to their limit values, B^* and λ_2^*, respectively. As in the first subsystem, the ratio of the slopes of the curves, $\lambda_{2,6}(A_6^*,B)$ and $\lambda_{2,7}(A_6^*,B)$, for $B=B_6^*$ gives the parameter scaling factor $\delta_{2,6}$ of level 6 in the second subsystem.

With increasing the level up to $n=15$, we first solve Eq. (27) and obtain the bicritical point (A_n^*,B_n^*) of level n and the pair of critical stability multipliers $(\lambda_{1,n}^*,\lambda_{2,n}^*)$ of level n. Next, we use the formulas of Eqs. (31) and (32) and obtain the parameter and orbital scaling factors of level n, respectively. These numerical RG results for the first and second subsystems are listed in Tables IV and V, respectively. Note that the accuracy in the numerical RG results is remarkably

TABLE V. Sequences of the critical point, the second critical stability multiplier, the parameter and orbital scaling factors, $\{B_n^*\}$, $\{\lambda_{2,n}^*\}$, $\{\delta_{2,n}\}$ and $\{\alpha_{2,n}\}$, in the second subsystem. For comparison, we also list the results obtained by a direct numerical method in the last row.

n	B_n^*	$\lambda_{2,n}^*$	$\delta_{2,n}$	$\alpha_{2,n}$
6	1.090 092 490 313	-1.177 467	2.395 07	-1.502 785
7	1.090 094 351 702	-1.178 671	2.393 58	-1.503 173
8	1.090 094 321 847	-1.178 625	2.393 59	-1.504 426
9	1.090 094 328 376	-1.178 649	2.393 10	-1.504 894
10	1.090 094 347 652	-1.178 820	2.392 80	-1.504 993
11	1.090 094 348 817	-1.178 844	2.392 81	-1.505 163
12	1.090 094 348 536	-1.178 830	2.392 78	-1.505 263
13	1.090 094 348 675	-1.178 847	2.392 74	-1.505 280
14	1.090 094 348 704	-1.178 856	2.392 73	-1.505 296
15	1.090 094 348 701	-1.178 853	2.392 73	-1.505 311
	1.090 094 348 701	-1.178 85	2.392 7	-1.505 318

improved with the level n and their limit values agree well with those obtained by a direct numerical method.

IV. SUMMARY

We have studied the scaling behavior of period doublings near the bicritical point, corresponding to a threshold of chaos in both subsystems. For this bicritical case, a type of non-Feigenbaum critical behavior appears in the second (response) subsystem, while the first (drive) subsystem is in the Feigenbaum critical state. Employing the truncation and eigenvalue-matching methods, we made the RG analysis of the bicritical behavior. For the case of the truncation method, we analytically obtained the fixed point, associated with the bicritical behavior, and its relevant eigenvalues. These analytic RG results are not bad as the lowest-order approximation. To improve the accuracy, we also employed the numerical eigenvalue-matching RG method, and obtained the bicritical point, the parameter and orbital scaling factors, and the critical stability multipliers. Note that the accuracy in the numerical RG results is improved remarkably with increasing the level n. Consequently, these numerical RG results agree well with the results obtained by a direct numerical method. Finally, note that this kind of bicritical behavior was also found in an electronic system [4] and in differential equations [6]. We thus believe that the bicriticality in the abstract system of unidirectionally coupled 1D maps may be observed in the real unidirectionally coupled systems.

[1] M. J. Feigenbaum, J. Stat. Phys. **19**, 25 (1978); **21**, 669 (1979).

[2] K. Kaneko, Phys. Lett. **111A**, 321 (1985); I. S. Aranson, A. V. Gaponov-Grekhov, and M. I. Rabinovich, Physica D **33**, 1 (1988); K. Kaneko, *ibid.* **68**, 299 (1993); F. H. Willeboordse and K. Kaneko, Phys. Rev. Lett. **73**, 533 (1994); F. H. Willeboordse and K. Kaneko, Physica D **86**, 428 (1995); O. Rudzick and A. Pikovsky, Phys. Rev. E **54**, 5107 (1996).

[3] J. H. Xiao, G. Hu, and Z. Qu, Phys. Rev. Lett. **77**, 4162 (1996); Y. Zhang, G. Hu, and L. Gammaitoni, Phys. Rev. E **58**, 2952 (1998); M. Hasler, Int. J. Bifurcation Chaos Appl. Sci. Eng. **8**, 647 (1998).

[4] B. P. Bezruchko, V. Yu. Gulyaev, S. P. Kuznetsov, and E. P. Seleznev, Dokl. Akad. Nauk (SSSR) **287**, 619 (1986) [Sov. Phys. Dokl. **31**, 268 (1986)].

[5] A. P. Kuznetsov, S. P. Kuznetsov, and I. R. Sataev, Int. J. Bifurcation Chaos Appl. Sci. Eng. **1**, 839 (1991); Physica D **109**, 91 (1997).

[6] A. P. Kuznetsov, S. P. Kuznetsov, and I. R. Sataev, Int. J. Bifurcation Chaos Appl. Sci. Eng. **6**, 119 (1996).

[7] J.-M. Mao and J. Greene, Phys. Rev. A **35**, 3911 (1987); S.-Y. Kim and H. Kook, Phys. Lett. A **178**, 258 (1993).

[8] B. Derrida, A. Gervois, and Y. Pomeau, J. Phys. A **12**, 269 (1979); B. Derrida and Y. Pomeau, Phys. Lett. **80A**, 217 (1980); B. Hu and J. M. Mao, Phys. Rev. A **25**, 1196 (1982); **25**, 3259 (1982); Phys. Lett. **108A**, 305 (1985); J. M. Mao and R. H. G. Helleman, Phys. Rev. A **35**, 1847 (1987); S.-Y. Kim and B. Hu, *ibid.* **41**, 5431 (1990).

[9] B. P. Bezruhko, Yu. V. Gulyaev, O. B. Pudovochkin, and E. P. Seleznev, Dokl. Akad. Nauk (SSSR) **314**, 332 (1990) [Sov. Phys. Dokl. **35**, 807 (1990)].

[10] R. S. MacKay, Ph.D. thesis, Princeton University, 1982; see Eqs. 3.1.2.12 and 3.1.2.13.

[11] O. E. Rössler, Phys. Lett. **71A**, 155 (1979).